2

A Field Robot with Rotated-claw Wheels

Ronggang Yue[1], Kai Li[1], Jun Du[1], Shaoping Wang[1],Jizhong Xiao[2]*
[1]*Beihang University*
China
[2]*City University of New York*
United States of American

1. Introduction

With the development of space science and technology, some countries have launched unmanned planetary exploration programs. Because planet surfaces are rough and formidable, planetary exploration rovers were used as a versatile and safe alternative to manned space missions to explore the planets. In recent years, many types of planetary rovers were developed including tracked type, legged type, and wheeled type, etc. (Li et al., 2005). Because wheeled rovers are well suited to provide smooth motion and offer a high payload capacity, they become the most popular and the mainstream in current rovers (Salemo et al., 2002).

In order to deal with the rough terrains of planetary surfaces, researchers put most of the efforts in designing new structure of rover body, but give less attention to new types of wheel. Currently, three main classes of wheels are used in planetary rovers as follows:

(1) Traditional Circular Wheel. Representations are the wheels of Mars exploration rover Spirit (Lindemann et al., 2006) developed by JPL and Japanese rover Micro5 (Takashi et al., 2003). This type of wheel has a circular shape with a lot of transverse striae spaced evenly around the wheel to increase the friction between ground and the wheel. The wheels are commonly used in most of the rovers that can move smoothly and turn around agilely. But its fatal disadvantage is that it can not scale the step whose height is larger than the radius of the wheel, also it can not cross the ditch whose width is larger than the diameter of the wheel.

(2) Flexible flake wheel. The representation is the wheel of Mars rover made by Toshiba in Japan (Liu et al., 2002). This kind of wheel is circular too, but the difference is that there are lots of flexible flake spaced evenly around the wheel. Compared with the first type wheel, this wheel increases buffering, and it can traverse over the step whose height is larger than the radius of the wheel. However, it can not cross the ditch whose width is larger than the diameter of the wheel.

(3) Multiple planetary wheel. A representative example is the wheel of Lunar rover developed by Harbin Institute of Technology (HIT) in China. The lunar rover uses planetary wheel which consists of three small circular wheels (Deng et al., 2003; Deng et al., 2004). When the lunar rover moves on flat terrain, only two small wheels touch ground. Once it encounters a big obstacle or step, the three small wheels revolve around the public center of

the wheels to traverse over the obstacle. This type of wheel overcomes the shortcomings of conventional circular wheels, and can climb over the step that is higher than diameter of the small wheel. However, this type of wheel makes the robot hard to make turns.
In this paper, we introduce a field robot (named as Rabbit) using the rotated-claw wheel have demonstrated the superiority over the conventional wheels. The analysis and testing results show that the innovative rotated-claw wheel can move steadily, turn around agilely, and climb the step whose height is larger than the radius of the wheel.

2. Design of the Rabbit

The basic requirements for an excellent field robot are motion stability, and strong capability of climbing obstacles or slopes. We designed a field robot prototype named as Rabbit whose motion is based on 4 rotated-claw wheels attached by "bogie levers" to the chassis. Figure1 shows its electrical diagram and Figure 2 shows the picture of the robot whose weight is 10.5Kg and outline dimension is 57cm×43cm×31cm. The body of Rabbit is mounted to the rocker through a differential mechanism. Rabbit is driven by 8 DC brushed motors that are controlled by a DSP controller. Each motor drives a series of stages of gearing that result in the final torque-speed relationship of the actuator. The total gear reduction rate for each actuator is 246:1. An encoder on each motor is utilized for sensing the rotation speed and determining steering angle. Under average load conditions, the wheel rotates at 24.4 rounds per minute, which results in a nominal vehicle speed of 15.3 cm/s with the 12 cm diameter wheels. In order to study the motion performance, an accelerator and an inclinometer are installed in the robot prototype.

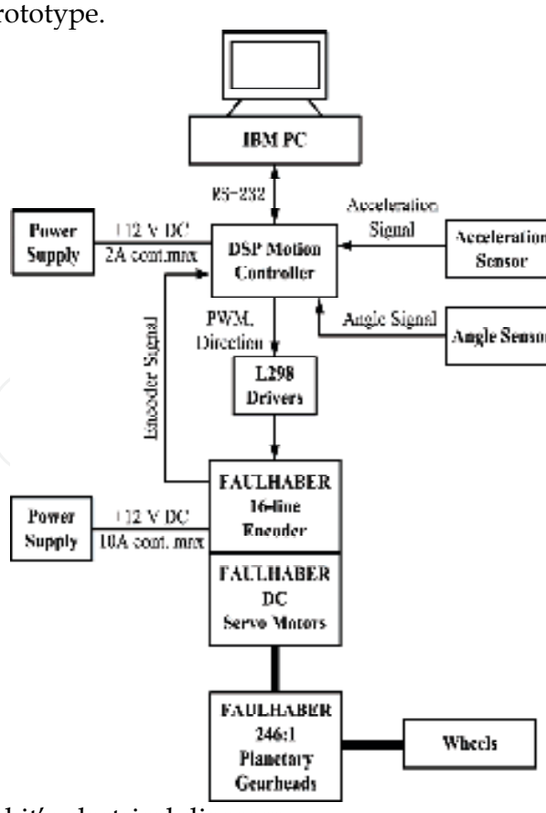

Fig. 1 Schematic of Rabbit's electrical diagram

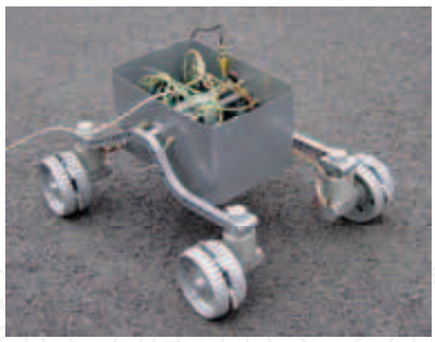

Fig.2 The field robot prototype named as Rabbit

Due to the rotated-claw wheel is an innovative. We would like to introduce principle and design of the wheel in detail.

3. Design of rotated-claw wheel

3.1 Principle of the rotated-claw wheel

The schematic diagram of the rotated-claw wheel is shown in Figure 3. In order to ensure the motion stability, turning flexibility, and obstacle-climbing capability, the wheel is designed as traditional circular structure with six sets of claw mechanism evenly installed around the wheel's outer skirt. Each set of claw mechanism consists of claw, claw axle, gag lever post and draught spring. Each claw can swing round its axle. The claw is in open state under the effect of draught spring and gap lever post when it doesn't touch the ground, and the claw swings into the wheel body under the effect of rover's weight when it touches the ground, which improves bumpy motion caused by hexagon effect.

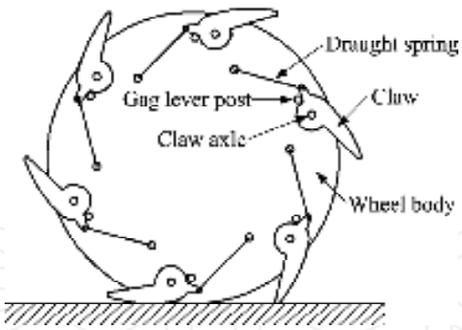

Fig. 3 Schematic diagram of the rotated-claw wheel

3.2 Motion stability analysis

As shown in figure 3, the claw can swing into the wheel body smoothly when the wheel rotates in anticlockwise direction, and the hexagonal effect of the wheel gives little influence on the stability of the rover. However, when the wheel rotates in clockwise rotation, the claw may disturb the stability of the wheel and cause the rover jounce. Therefore, we must analyze the stress of the wheel and select design parameters carefully to avoid this problem in the case of clockwise rotation.

When design the wheel, we first determine the claw dimensions and the distance between each claw axle and wheel's center, then adjust the position of gag lever post. Figure 4 shows the process of a claw touching ground when the wheel rotates in clockwise direction on flat terrain. There are two cases about angle γ in Figure 4. One is the case when angle γ is larger than 90°, the other is the case when angle γ is less than 90°. We will discuss the two cases respectively.

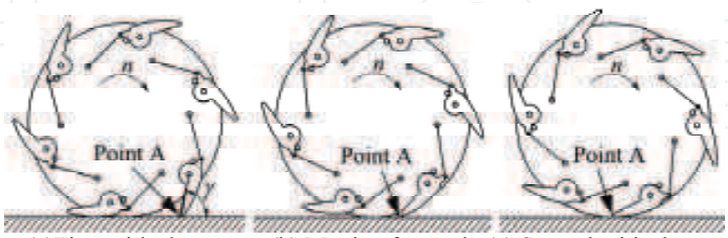

(a)First critical state (b) Moving forward (c) Second critical state

Fig. 4 Rotation in clockwise direction on flat terrain of rotated-claw wheel

3.2.1 When angle γ is larger than 90°

Figure 5(a) shows the critical state when a claw tip touches the ground while the wheel leaving the ground. At this time instance only point *A* supports the wheel, i.e., only point *A* gets supporting force from the ground. Taking the claw touching the ground as an object, we can get the stress analysis shown in Figure 5(b), in which the wheel and the claw are expressed in dashed lines and the claw is simplified as line segments *AOB* and the draught spring is simplified as line *BC*.

Stress analysis in Figure 5(b) shows that the claw satisfies the following equation:

$$Nl_1 \sin\alpha + fl_1 \cos\alpha + Fl_2 \cos\beta = N_1 l_3 \tag{1}$$

Where, N is the acting force of ground to wheel at point A; N_1 is the acting force of gag lever post to claw; l_1 is the length of line OA; l_2 is the length of line OB; l_3 is the level distance of force N_1; a is the angle between line OA and plumb line; β is the angle between line OB and the line perpendicular to line BC; f is the friction between point A and ground; F is the pre-setting pulling force of spring BC.

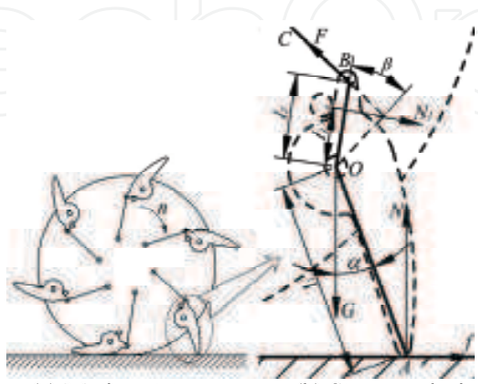

(a) Motion state (b) Stress analysis

Fig. 5 Stress analysis when angle γ is larger than 90°

Because it is in the balance state, the claw can not swing around point O when angle γ is larger than 90°, and the claw can not swing into the wheel body. Now we get the first condition ensuring the claw swing into the wheel body smoothly is that angle γ must be less than 90°. We can adjust numerical values of l_1, l_2, l_3, a, β to make γ be less than 90°.

3.2.2 When angle γ is less than 90°

There are two critical states as illustrated in Figure 4(a) and Figure 4(c).

(1) First critical state

Figure 6 shows the first critical state-when the wheel is on the point of leaving the ground, in which a claw tip touches the ground, and its weight acts on point A. At this time instance, only point A supports the wheel. Taking the claw touching the ground as an object, we can get the stress analysis shown in Figure 6(b), in which the wheel and the claw are expressed in dashed lines, the claw is simplified as line segments AOB and the draught spring is simplified as line BC.

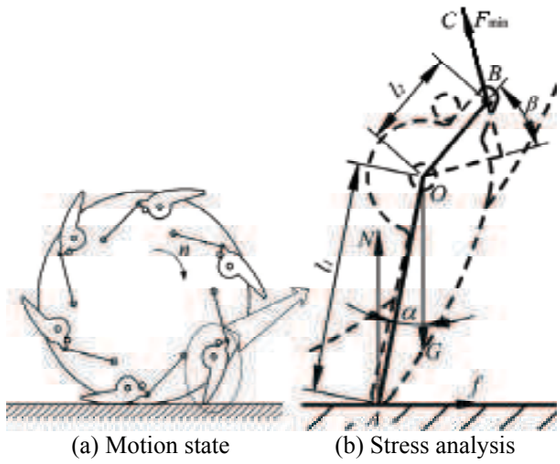

(a) Motion state (b) Stress analysis

Fig. 6 Stress analysis at the first critical state

In Figure 6, the claw touching the ground must swing around the point O clockwise if the wheel is to rotate clockwise smoothly. In order to satisfy this requirement, every claw must satisfy the following equations:

$$\begin{cases} Nl_1 \sin\alpha > F_{\min} l_2 \cos\beta + fl_1 \cos\alpha \\ N \approx G \\ F_{\min} = k\Delta x_{\min} \\ f = \mu N \end{cases} \tag{2}$$

Where, N is the acting force of ground to wheel at point A; l1 is the length of line OA; l_2 is the length of line OB; a is the angle between line OA and plumb line; β is the angle between line OB and the line perpendicular to line BC; $F_{\min}$ is the pre-setting pulling force of spring BC; f is the friction between point A and ground; G is the gravity force acting on the single wheel from the rover that is approximate to N; k is the elastic coefficient of spring BC; $\Delta x_{\min}$

is the extension of spring *BC*; μ is the coefficient of sliding friction between point *A* and ground.

Then we can get the following inequation:

$$Gl_1 \sin\alpha > k\Delta x_{\min} l_2 \cos\beta + \mu G l_1 \cos\alpha \tag{3}$$

Inequation (3) is the first criterion that makes the claw swing into the wheel body freely and ensures the wheel rotate clockwise smoothly.

(2) Second critical state

The second critical state is shown in Figure 7(b), when the excircle of the claw is tangent to the road surface, in which its weight acts on point *A* and the other part of the wheel doesn't touch the ground.

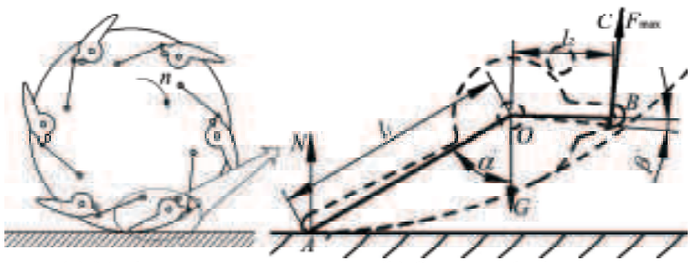

(a) Motion state (b) Stress analysis

Fig. 7 Stress analysis at the second critical state

In Figure 7, the claw must be inside of the profile of the wheel body if the wheel is to rotate clockwise smoothly. Every claw must satisfy the following equations:

$$\begin{cases} F_{\max} l_2 \cos\beta' < N l_1 \sin\alpha' \\ N \approx G \\ F_{\max} = k\Delta x_{\max} \end{cases} \tag{4}$$

Where, F_{max} is the pulling force of spring *BC*; l_1 is the length of line *OA*; l_2 is the length of line *OB*; a' is the angle between line *OA* and plumb line; β' is the angle between line *OB* and the line perpendicular to line *BC*; *N* is the acting force of ground to wheel at point *A*; *G* is the gravity force of the single wheel; *k* is the elastic coefficient of spring *BC*; $\Delta x_{\max}$ is the extension of spring *BC*.

Then we can get the following inequation:

$$k\Delta x_{\max} l_2 \cos\beta' < G l_1 \sin\alpha' \tag{5}$$

Inequation (5) is the second criterion that makes the claw swing into the wheel body freely and ensures the wheel rotate clockwise smoothly.

In summary, when designing the rotated-claw wheel, the distance between point *O* and the center of the wheel should be chosen appropriately. When the claw touches the ground, the angle γ should be less than 90° as shown in Figure 5(a). At the same time, appropriate numerical values of *G*, l_1, l_2, *a*, β, a', β', $\Delta x_{\min}$, $\Delta x_{\max}$ should be chosen to satisfy inequations (3) and (5). These criteria ensure the wheel rotate in clockwise direction reposefully and reduce jounce (Yue et al., 2007).

3.3 Obstacle-climbing analysis

Conventional circular wheels can not scale the step whose height is larger than the radius of the wheel. In Figure 8, the step height is H_1, and the radius of the conventional circular wheel is R. If the wheel wants to traverse over the step, H_1 must be less than R. The rotated-claw wheel overcomes this shortcoming. In Figure 9, the step height is H_2, and the radius of the rotated-claw wheel is still R. However, due to the existence of the claw, wheel can scale the step whose height is larger than the radius of the wheel by h, and h can be designed larger than zero by choosing suitable numerical values of l_1, l_2, a, β, and distance between point O and wheel's center. From the analysis, we can claim with confidence that the obstacle-climbing capability of the rotated-claw wheel is improved in comparison with the conventional circular wheels. Real experimental results will verify the performance.

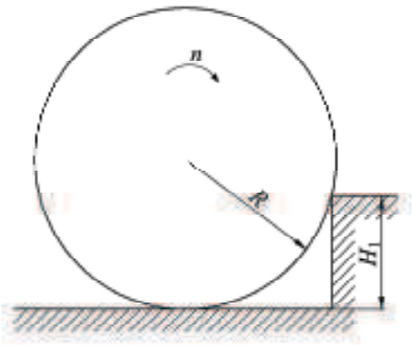

Fig. 8 Sketch drawing of circular wheel climbing a step

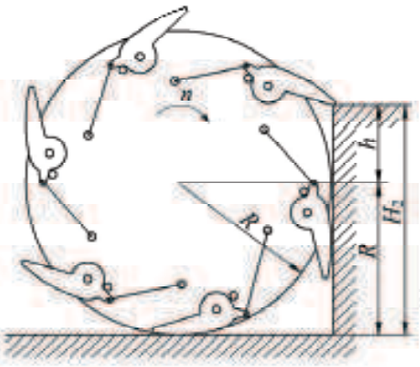

Fig. 9 Sketch drawing of rotated-claw wheel climbing a step

3.4 Structure design of rotated- claw wheel

Based on the criteria mentioned above, this paper designed the three-dimensional model of the rotated-claw wheel shown in Figure 10 that includes a steering mechanism and the obstacle-climbing mechanism (rotated-claw). In order to enhance the friction between the wheel and ground, grooves are constructed around the wheel in even space. The deigned diameter of the wheel is 120 mm and its width is 60 mm. Dimensions of the claw is shown in Figure 11, which make γ be less than 90°.

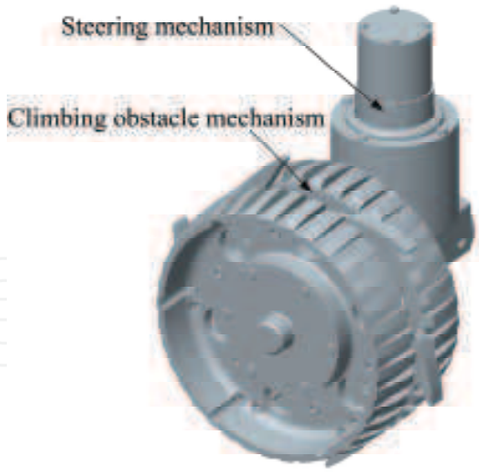

Fig. 10 Three-dimensional model of the rotated-claw wheel

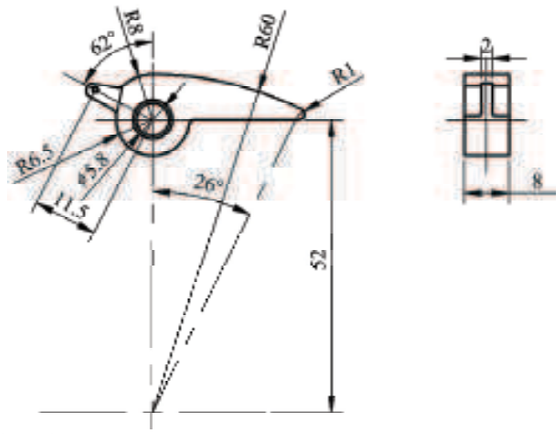

Fig. 11 Dimensions of the claw

4. Performance test of Rabbit

In order to test environmental adaptability of Rabbit, the experiments are conducted on various terrain, including surfaces of bituminous macadam, dry soil, step, slope, and simulated lunar soil. All of the data were collected at maximum velocity.

4.1 Motion stability performance

The motion stability analysis reveals that the six claws may cause a little jounce when the rotated-claw wheel rotates in clockwise direction, while smooth motion is guaranteed in anticlockwise rotation. We conducted experiments to evaluate the motion stability performance by commanding the Rabbit robot move on flat ground of bituminous macadam. Figure12 shows the acceleration curve of Rabbit in plumb direction when the rotated-claw wheels rotate in clockwise direction. The acceleration varies from -0.39g to 0.46g. Figure 13 gives the acceleration curve of Rabbit in plumb direction when the wheels make anticlockwise rotation, it shows that the acceleration changes from -0.13g to 0.16g. Figure14 gives the acceleration curve in plumb direction when Rabbit rotates with the claws

retracted inside the wheel body (Now the rotated-claw wheel is the same as conventional circular wheel). It shows that the acceleration varies from -0.13g to 0.13g. Compare Figure13 with Figure14, we can see that stability of the rotated-claw wheel under the condition of retracted claws is similar to that of conventional circular wheel.

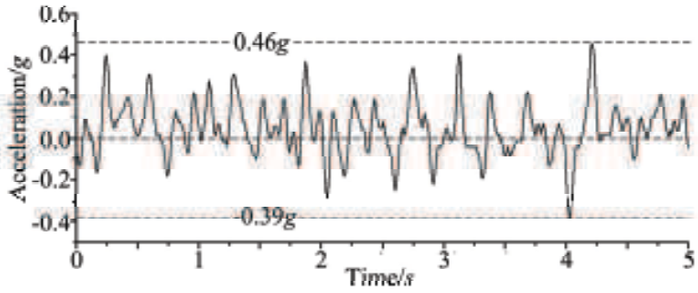

Fig. 12 Plumb direction acceleration curve of Rabbit when the rotated-claw wheels make clockwise rotation on bituminous macadam ground

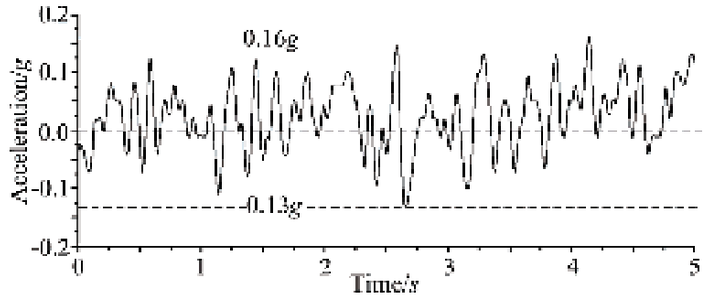

Fig. 13 Plumb direction acceleration curve of Rabbit when the rotated-claw wheels make anticlockwise rotation on bituminous macadam ground

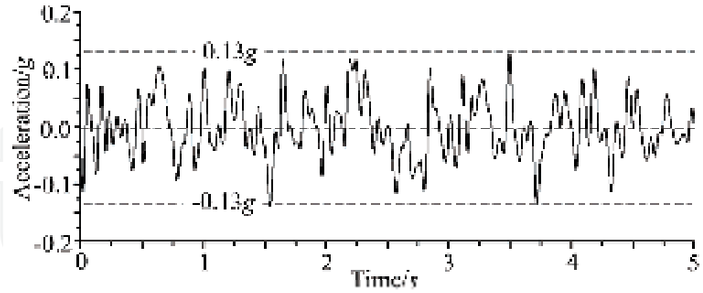

Fig. 14 Plumb direction acceleration curve of Rabbit when the rotated-claw wheels rotate with retracted claws on bituminous macadam ground

It is obvious that the motion stability under anticlockwise rotation is more stable than that under clockwise rotation. The reason is that the claw can swing into the wheel body under anticlockwise rotation while the hexagon effect causes the bumpiness under clockwise rotation. So the Rabbit should be commanded to move in a backward mode (i.e., all the wheels rotate in anticlockwise direction) on flat hard ground.

4.2 Performance of climbing obstacles

4.2.1 Dry soil terrain

In order to test Rabbit's motion performance on dry soil terrain with multi-obstacle, we did another experiment as shown in Figure15. Figure16 shows the acceleration curve of Rabbit in plumb direction that denotes the acceleration varying from -0.125g to 0.125g. Figure17 gives the acceleration curve of Rabbit in plumb direction on dry soil when the wheels rotate in clockwise direction. It shows that the acceleration varies from -0.10g to 0.10g. Figure18 gives the acceleration curve of Rabbit in plumb direction on dry soil when the Rabbit moves under the condition of retracted claws, which shows the acceleration varies from -0.10g to 0.10g. Compare Figure17 with Figure18, we can see that stability of the wheel is as good as conventional circular wheel under the condition of retracted claws.

It is obvious that the backward mode is smoother than forward mode (i.e., all the wheels rotate in clockwise direction) when Rabbit operates on dry soil. But the two results are approximative. The reason is that the claw can sink into soil and the obstacle-climbing capability is enhanced. So Rabbit should move in a forward mode when operates on dry soil terrain with multi-obstacle. The highest obstacle on dry soil terrain that the robot can climb over is 13cm. The experiments also show that Rabbit can step over the clod or stone whose dimension is equivalent to the diameter of the wheel.

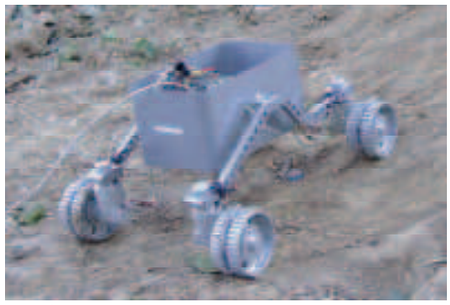

Fig. 15 Rabbit moves on dry soil terrain

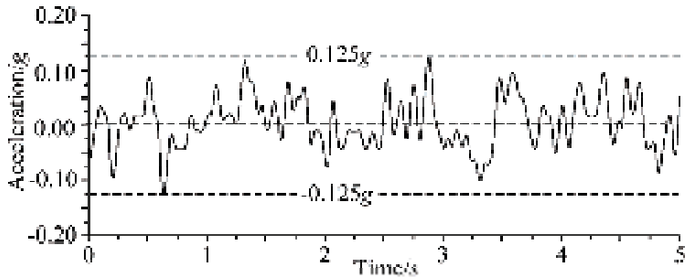

Fig.16 Plumb direction acceleration curve of Rabbit while the robot moves forward on dry soil terrain

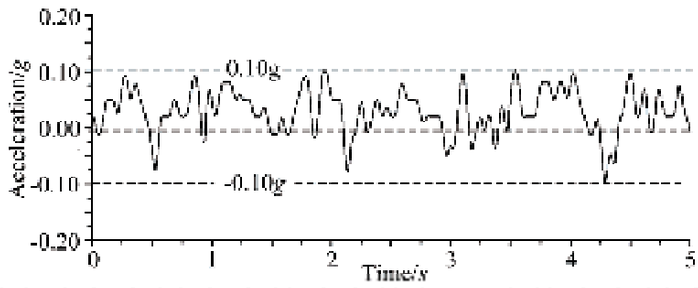

Fig. 17 Plumb direction acceleration curve of Rabbit while the robot moves backward on dry soil terrain

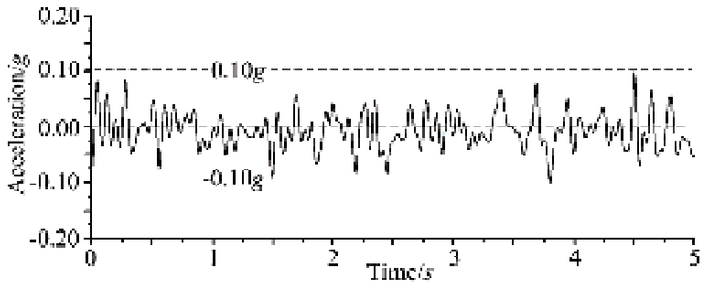

Fig. 18 Plumb direction acceleration curve of Rabbit while wheels rotates under the condition of retracting claws on dry soil terrain

4.2.2 Step terrain

When the robot moves on steps terrain, Rabbit should move in a forward mode (i.e., all the wheels rotate in clockwise direction), because the claw can catch step in front of the wheel and help the robot to climb over it easily in the forward mode. Table 1 shows the experimental results in different step height.

Step height/cm	2.2	3.9	6.3	8.1	9.0
Result	Success	Success	Success	Success	Fail

Table 1. Experimental results on different height step

It is obvious that the rotated-claw wheel can climb over the 8.1cm step that is almost 1.35 times of wheel's radius as shown in Figure19. This verifies that the rotated-claw wheel can improve the obstacle-climbing capacity.

Fig.19 Climbing step in a forward mode

4.2.3 Slope terrain

In order to test Rabbit's motion performance on slope terrain, we did other experiments as shown in Figure20, in which the Rabbit climbs over slope terrain in a forward mode.

Fig. 20 Rabbit climbs over slope terrain in a forward mode

Figure 21 and Figure 22 show the angle curve when Rabbit climbs slope terrain in forward mode and backward mode respectively. We can see that Rabbit can climb a slope up to 40° in the forward mode, in contrast, Rabbit is able to climb a slope just up to 31° in backward mode.

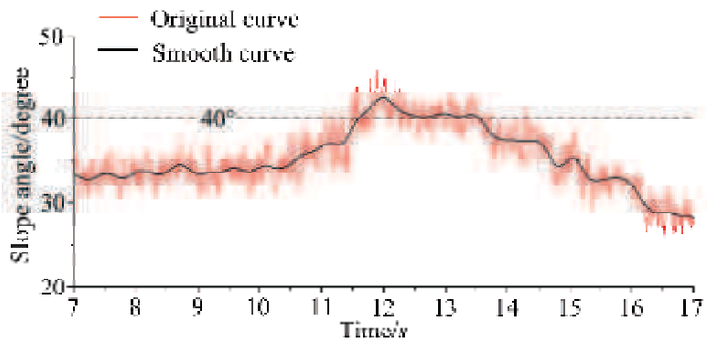

Fig.21 Angle curve when Rabbit climbs slope terrain in forward mode

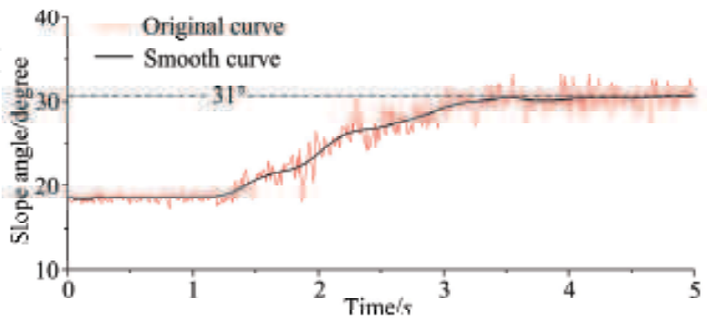

Fig.22 Angle curve when Rabbit climbs slope terrain in backward mode

Comparing Figure21 and Figure22, the rotated-claw wheel increases the climbing slop angle up to 9 degree. The reason is that the claw can sink into soil in motion, which enhances physical attraction between the wheel and ground. So Rabbit should move in a forward mode when it moves on slope terrain.

4.2.4 Lunar soil simulation

In order to adapt to the utilization in planetary, we did experiments on simulated terrain of lunar soil whose material is pozzuolana. The lunar soil is loaded in a trough which has dimensions of 300cm×80cm×60cm as shown in Figure 23. Void ratio (It is defined as the ratio of the volume of all the pores in a material to the volume of all the grain) of the lunar soil is approximately from 0.8 to 1.0, and density of the grain is 2.77g/cm3.

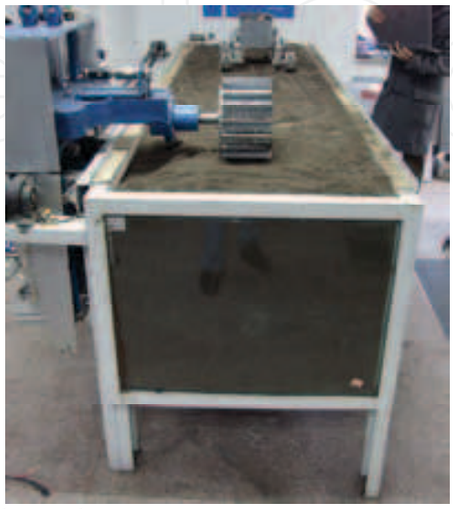

Fig. 23 Trough for lunar soil simulation

We tested Rabbit's motion performance on rough terrain and multi-obstacle terrain made up of lunar soil as shown in Figure24 and Figure25. The result shows that Rabbit can move freely on simulated lunar soil.

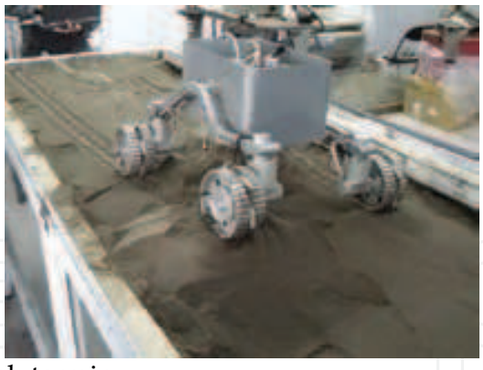

Fig.24 Experiment on rough terrain

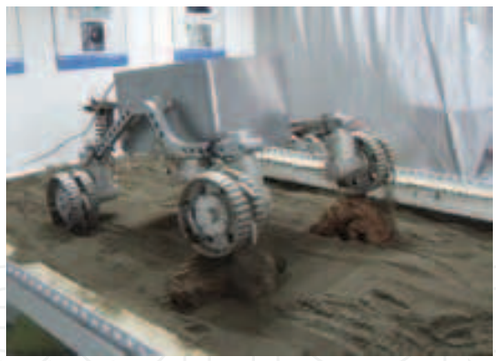

Fig.25 Experiment on multi-obstacle terrain

In addition, we tested Rabbit's horizontal pulling capacity on simulated lunar soil in both forward and backward modes (Figure 26). The experimental results show that Rabbit can generate maximum pulling forces of 26.5N in forward mode, and 25.1N in backward mode.

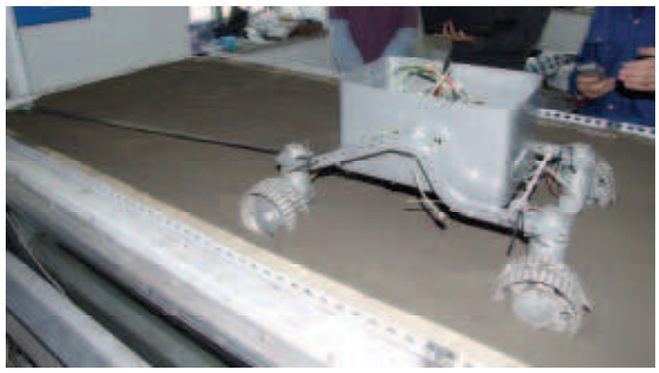

Fig. 26 Rabbit's horizontal pull testing

5. Performance comparison

According to the available data from literature, we compare the performance of Rabbit with MFEX and Spirit robots. MFEX (Microrover Flight Experiment) was a small rover designed by JPL (Jet Propulsion Laboratory) in 1990s. It was launched to Mars in December 1996 [9]. Spirit is one of the latest Mars rovers designed by JPL. It landed on Mars on January 4, 2004 [10], and finished exploration mission with flying colors in the following years (and still alive). Table 2 lists the data comparison among Rabbit, MFEX, and Spirit. From the table, we can see that maximum slope the Rabbit can climb is larger than that of the other two rovers although Rabbit only equipped with 4 rotated-claw wheels (2 wheels less than the other rovers). In addition, Rabbit can climb over step which is higher than the radius of wheel.

Robot name	Rabbit	MFEX	Spirit
Mass	10.5Kg	9Kg	176.5Kg
Dimensions	57 cm×43 cm×30.9cm	63 cm×48 cm×28cm	140 cm×120 cm×150cm
Chassis type	Body mounted to rocker through a differential	Body mounted to rocker through a differential	Body mounted to rocker through a differential
Suspension system	Springless suspension	Springless suspension	Rocker-bogie suspension
Locomotion system	4 wheels (four steerable)	6 wheels (outer four	6 wheels (outer four

		steerable)	steerable)
Maximum speed	0.153m/s	0.02m/s	0.046m/s
Operational range	1Km	10m	1Km
Layout of wheels	Claw-wheel with 120 mm diameter 60 mm width	wheels with 130 mm diameter 60 mm width	250 mm diameter
Motion control processors	One 2407A DSP	One Intel 80C85	
Max. step height	13cm (Can climb over the step whose height is 1.35 times higher than the radius of the wheel)	Less than 6.5cm	Less than 12.5cm
Maximum slope	40 ° in forward mode, 31 ° in back mode (in soft soil)	32 ° (dry sand) 17 ° (lunar soil simulant)	16 ° at least 30 ° in the nature of the Mars soil and terrain

Table 2. Performance comparison of Rabbit, MFEX, and Spirit

6. Conclusion

In this paper, we introduce a field robot using the rotated-claw wheel that has strong capacity of climbing obstacles. The experimental results demonstrate that Rabbit can move in different terrain smoothly and climb over step of 8.1cm and slop of 40°. The Rabbit can adopt different moving modes on different terrains.

(1) Rabbit should move in backward mode on flat hard ground.

(2) Rabbit should move in forward mode on rough, slop, and step terrains.

Because the rotated-claw wheel overcomes the disadvantages of conventional mobile robot wheels, it provides a better solution for field and planetary robots.

7. Acknowledgment

We thank Wen Li, Gang Sun, and Peng Sun of Beihang University for their valuable help in the experiments of lunar soil simulation.

8. References

Cuilan Li; Peisun Ma; Xueguan Gao & Zhikui Cao. (2005). A new six-wheel lunar robot for uneven surface. *Drive System Technique*, Vol. 19, No. 1, (Mar. 2005) page numbers(9-13), 1006-8244 (in Chinese)

Alessio Salemo; Svetlana Ostrovskaya & Jorge Angeles. (2002). The Development of Quasiholonomic Wheeled Robots, *Proceedings of the 2002 IEEE nternational Conference on Robotics and Automation*, Vol.4 , pp. 3514 – 3520, Washington, DC, May. 2002.

Randel A. Lindemann; Donald B. Bickler; Briand. Harrington; Gary M. Ortiz & Christopher J. Voorhees. (2006). Mars exploration rover mobility development. *Robotics & Automation Magazine*, IEEE, Vol. 13, No. 2, (Jun. 2006) page numbers (19-26), 1070-9932.

Takashi Kubota; Yoji Kuroda; Yasuharu Kunii & Ichiro Nakatani. (2003). Small, light-weight rover Micro5 for lunar exploration. *Acta Astronautica*, Vol. 52, No. 2-6, (Jan.-Mar. 2003) page numbers (447-453), 0094-5765.

Fanghu Liu; Jianping Chen; Peisun Ma & Zhikui Cao. (2002). RESEARCH STATUS AND DEVELOPMENT TREND TOWARDS PLANETARY EXPLORATION ROBOTS. *Robot*, Vol. 24, No. 3, (May. 2002) page numbers (268-275), 1002-0446. (in Chinese)

Zongquan Deng; Haibo Gao; Ming Hu & Shaochun Wang. (2003). Design of lunar rover with planetary wheel for surmount obstacle. *Journal of Harbin Institute of Technology*, Vol. 35, No. 2, (Feb. 2003) page numbers (203-213), 0367-6234. (in Chinese)

Zongquan Deng; Haibo Gao; Shaochun Wang & Ming Hu. (2004). Analysis of climbing obstacle capability of lunar rover with planetary wheel. *Journal of Beijing University of Aeronautics and Astronautics*, Vol. 30, No. 13, (Mar. 2004) page numbers (197-201), 1001-5965. (in Chinese)

Ronggang Yue; Shaoping Wang; Zongxia Jiao & Rongjie Kang. (2007). Design and performance simulation of a new type wheel with claws. *Journal of Beijing University of Aeronautics and Astronautics,* Vol. 33, No. 12, (Dec. 2007) page numbers (1408-1411), 1001-5965. (in Chinese)

K. Schilling & C. Jungius. Mobile robots for planetary exploration. (1996). *Control Engineering Practice*, Vol. 4, No. 4, (Apr. 1996) page numbers (513–524), 0967-0661. (in Chinese)

Glenn Reeves & Tracy Neilson. (2005). The Mars Rover Spirit FLASH Anomaly. *Aerospace Conference*, 2005 IEEE, pp. 4186-4199, Mar. 2005.

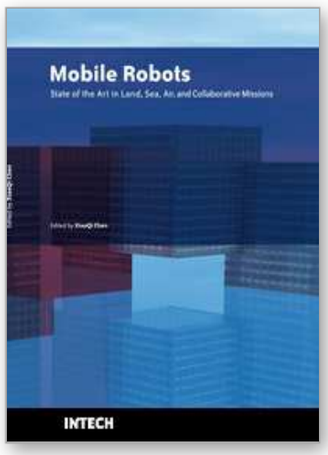

Mobile Robots - State of the Art in Land, Sea, Air, and Collaborative Missions

Edited by XiaoQiChen

ISBN 978-953-307-001-8
Hard cover, 335 pages
Publisher InTech
Published online 01, May, 2009
Published in print edition May, 2009

Since the introduction of the first industrial robot Unimate in a General Motors automobile factory in New Jersey in 1961, robots have gained stronger and stronger foothold in the industry. In the meantime, robotics research has been expanding from fix based robots to mobile robots at a stunning pace. There have been significant milestones that are worth noting in recent decades. Examples are the octopus-like Tentacle Arm developed by Marvin Minsky in 1968, the Stanford Cart crossing a chair-filled room without human assistance in 1979, and most recently, humanoid robots developed by Honda. Despite rapid technological developments and extensive research efforts in mobility, perception, navigation and control, mobile robots still fare badly in comparison with human abilities. For example, in physical interactions with subjects and objects in an operational environment, a human being can easily relies on his/her intuitively force-based servoing to accomplish contact tasks, handling and processing materials and interacting with people safely and precisely. The intuitiveness, learning ability and contextual knowledge, which are natural part of human instincts, are hard to come by for robots. The above observations simply highlight the monumental works and challenges ahead when researchers aspire to turn mobile robots to greater benefits to humankinds. This book is by no means to address all the issues associated mobile robots, but reports current states of some challenging research projects in mobile robotics ranging from land, humanoid, underwater, aerial robots, to rehabilitation.

InTech Europe
University Campus STeP Ri
Slavka Krautzeka 83/A
51000 Rijeka, Croatia
Phone: +385 (51) 770 447
Fax: +385 (51) 686 166

InTech China
Unit 405, Office Block, Hotel Equatorial Shanghai
No.65, Yan An Road (West), Shanghai, 200040, China
中国上海市延安西路65号上海国际贵都大饭店办公楼405单元
Phone: +86-21-62489820
Fax: +86-21-62489821

IntechOpen

IntechOpen